# Magneto-electric coupling at metal surfaces

L. Gerhard, T. K. Yamada, T. Balashov, A. F. Takács, R. J. H. Wesselink,
M. Däne, M. Fechner, S. Ostanin, A. Ernst, I. Mertig, and W. Wulfhekel

## HYDROGEN ADSORPTION

Biedermann et al. [1] found an influence of hydrogen adsorption on the crystallographic structure of the two phases. To make sure that our experiments were carried out without the influence of residual hydrogen gas, we did the following: Firstly, we checked the number of hydrogen atoms adsorbed on a clean Pt surface in the same experimental setup. On this surface, individual hydrogen atoms can easily be imaged with STM. Using this data, an adsorption rate of 1.3 hydrogen atoms per 1000 $nm^2$ per hour was found. Since the sticking coefficient $S$ of hydrogen on Fe [2] is lower ($S = 0.1$) than that on Pt [3] ($S = 0.95$) and the reported switching was observed about 20 hours after sample preparation, the estimated contamination in this experiment is only one hydrogen atom per island (100 $nm^2$).

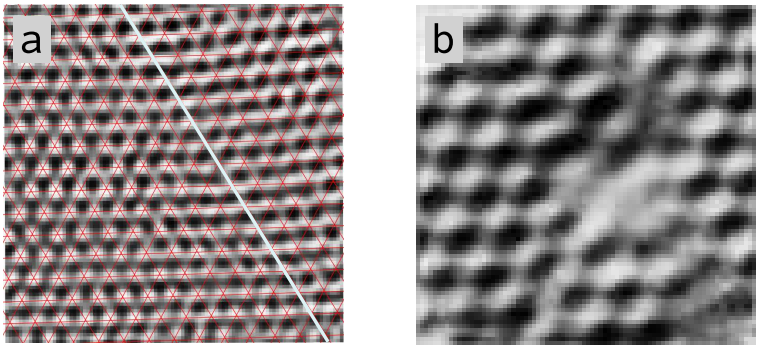


FIG. 1: a)Atomically resolved structure of a bilayer Fe island on Cu(111) (3.7×3.7 $nm^2$). The tunnelling parameters are 60 mV and 6 nA. The red grid shows the hexagonal lattice of the fcc structure on the left hand side. The atomic lines of the bcc phase on the right hand side are misaligned by about 5 °. The white line indicates the domain boundary. b) After exposure to 2 L of $H_2$ (purity 99.999%) the atomic structure changes: an STM picture of the same size as in a) clearly shows a hydrogen induced superstructure.

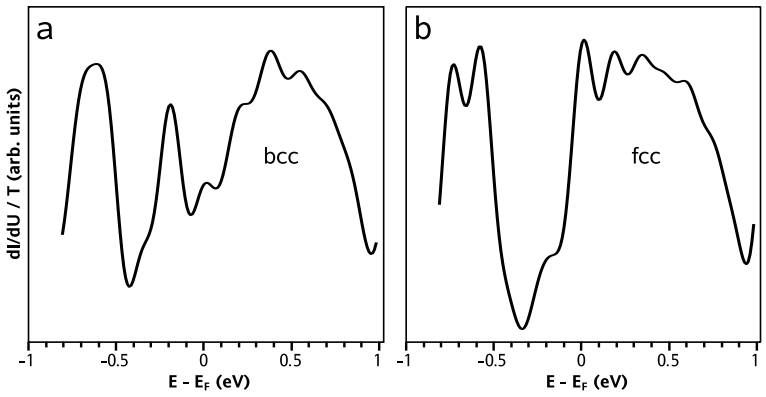


FIG. 2: Normalised differential conductance spectra of the bcc (a) and the fcc (b) phase after exposure to 2 L $H_2$.

Secondly, the Fe/Cu(111) sample was exposed to a dose of 2 L hydrogen. After adsorption of hydrogen the atomic structure of the surface drastically changed. High resolution STM shows a (2x2) superstructure of the Fe surface (see Fig. 1b), that we never observed on a clean sample (see Fig. 1a). Furthermore, $dI/dU$ spectra on the H covered Fe islands look different from those obtained on clean samples (see Fig. 2). Thus, hydrogen covered surfaces can be easily distinguished from clean surfaces.

These findings exclude hydrogen adsorption and desorption as the origin of the observed reversible phase transition.

## PULSE LENGTH LIMIT

In Fig. 3 we show that it is possible to induce a transition even with pulses as short as 60 $\mu$s (shorter pulse lengths could not be achieved by our equipment). The black line display the gap voltage as function of time, the coloured line displays the z-position of the STM tip as measured with a fast oscilloscope. The pulse width is only 60 $\mu$s (see inset). During the pulse, the feed back loop was opened and stayed open until 7 ms after the pulse to relax the I-V converter (bandwidth 7 kHz). When closing the feed back loop, the tip moves 12 pm down indicating the phase transition. The speed of this movement is limited by the cut-off frequency of the feed back loop.

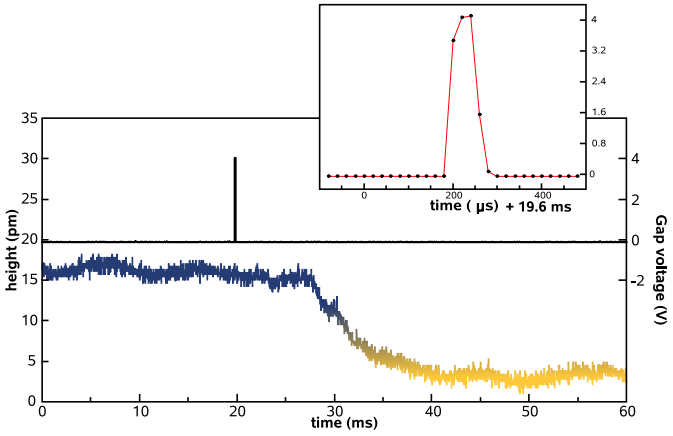


FIG. 3: Applied gap voltage (black line) and measured height (coloured line) at fixed tip position when applying a pulse of 60 $\mu$s (see inset).

## CURRENT DISTANCE RELATION

The current $I$ in a tunnelling junction depends exponentially on the distance $d$ and the square root of the apparent barrier height $\Phi$ according to Simmons' rule for tunnelling: $I = \frac{U}{12.9k\Omega} \cdot e^{\frac{-2\cdot\sqrt{2m\Phi}}{\hbar}\cdot d}$ [4]. For zero distance a point contact resistance of 12.9 k$\Omega$ was assumed, $U$ being the gap voltage. In order to measure the apparent barrier

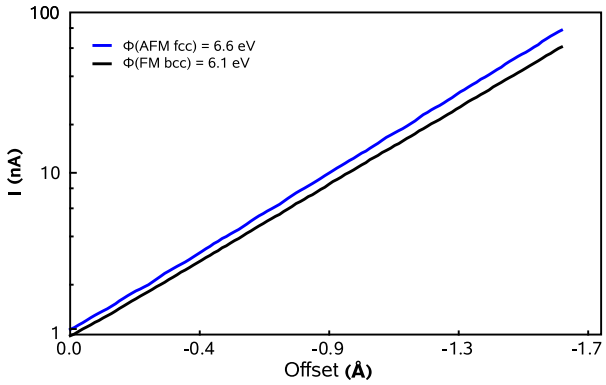


FIG. 4: Logarithmic plot of the tunnelling current as function of an offset to distance between tip and sample. At constant gap voltage the tunnelling current depends exponentially on the offset. The two different phases on the Fe islands show two different apparent barrier heights.

height, we recorded the tunnelling current as function of the distance between tip and sample at a constant gap voltage. We switched off the feed back loop. By applying an additional voltage to the z-piezo it can be elongated in a controlled way narrowing the tunnelling gap between tip and sample. During this we record the tunnelling current. In a logarithmic plot (Fig. 4) we find a linear dependence. From fits of the slope we obtain the barrier

height. By measuring several $I-d$ curves on different Fe islands both in the antiferromagnetic fcc centre and on the ferromagnetic bcc rim we obtained $\Phi_{AFM} = 6.6\,\mathrm{eV}$ and $\Phi_{FM} = 6.1\,\mathrm{eV}$.

## FIRST-PRINCIPLES CALCULATIONS

### Total energy landscape without an applied electric field

We investigated the total energy landscape of 2 ML Fe on Cu(111) as function of the interlayer distance between the Fe layers and the lateral displacement of the top Fe atoms. The interlayer distance $d_s$ was varied between 0.9 and 1.05 times the copper interlayer distance $d_{Cu}$ and the lateral position of the top Fe atoms between the threefold hollow site position (fcc) and the bridge position (bcc) as depicted in Fig. 5a-c. The total energy of ferromagnetic and antiferromagnetic states were computed and the lowest energy state was identified as the antiferromagnetic fcc state with an interlayer distance of 0.91 $d_{Cu}$. For a given position of the topmost Fe layer, we determined the magnetic state of lower energy and plot the energy difference of this state with respect to the overall ground state. This difference is plotted in (Fig. 5d). In the absence of an electric field, the compressed antiferromagnetic fcc state is most stable (lower left corner). A second but metastable state is the ferromagnetic bcc state with a interlayer distance of about 0.97 $d_{Cu}$. Both states are separated by a large energy barrier of 160 meV.

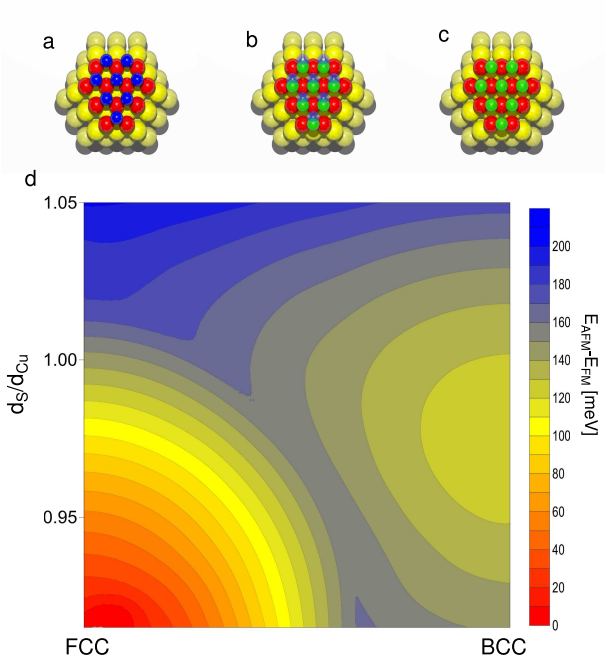


FIG. 5: The fcc-to-bcc transformation of the surface layer in Fe/Cu(111). (a) Top view of fcc stacking. The yellow balls indicate the Cu fcc (111) substrate. Red and blue balls represent Fe atoms on the interface and surface, respectively. (b) Lateral atomic movement from fcc (blue) to bcc (green) stacking. The surface atoms move laterally from the fcc positions crossing the low energetic barrier by thermal excitations and pass to the energetically favoured bcc structure. (c) Top view of the bcc stacking of the Fe/Cu(111) surface. (d) Total energy difference between the antiferromagnetic global ground state and the magnetic ground state upon vertical and lateral movements of surface atoms during fcc-to-bcc transition in Fe/Cu(111) from first-principles calculations. The horizontal axis represents the lateral migration of Fe surface atoms from fcc (111) to bcc (110) positions. The vertical axis shows the vertical movement of Fe surface atoms in form of the surface interlayer distance $d_S$ normalised by the Cu interlayer distace $d_{Cu}$.

A field induced transition between the states can to first order be explained by a field induced change of the interlayer distance which in turn reduces the energetic barrier between the states. To higher orders, the barriers for field induced transitions have been calculated including also the electronic effects as shown in the main paper and discussed in the following.

Since the structural deformations of the Fe/Cu(111) surface in the experiment are mainly induced by the electric

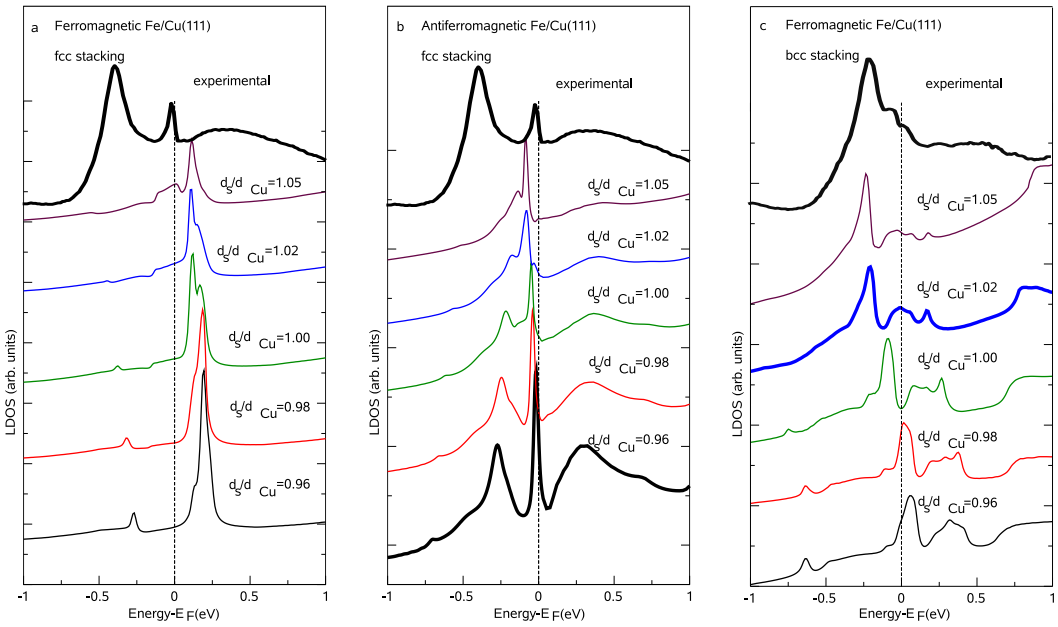


FIG. 6: Scanning tunnelling spectroscopy measurements in comparison with first principles calculations of the LDOS for different magnetic scenarios. Three possible configurations were considered: (a) Ferromagnetic fcc, (b) Antiferromagnetic fcc and (c) Ferromagnetic bcc stacking. Additionally different surface interlayer distances for each configuration were considered. The differential conductance spectrum obtained on the fcc phase does not fit the calculated LDOS for the ferromagnetic fcc stacking irrespective of the interlayer distance. It only agrees with the calculated LDOS for an antiferromagnetic configuration, in particular for an interlayer distance of $d_s = 0.96 d_{Cu} = 2.00$ Å. The experimental spectrum on the bcc phase agrees best with the theoretical LDOS for the ferromagnetic configuration and an interlayer distance of $d_s = 1.02 d_{Cu} = 2.12$ Å.

field, the conventional ground state calculations cannot provide adequate relaxations of atomic position in this system. Therefore, the crystal, electronic and magnetic structures of the Fe/Cu(111) system were determined from a direct comparison of the calculated LDOS and experimental scanning tunnelling spectra. For this we traced the LDOS through various structural and magnetic configurations so long until agreement with the experiment was achieved.

We started our simulations assuming Fe layers in fcc stacking ordered ferromagnetically to each other. The LDOS, corresponding to several interlayer distances, are shown in Fig. 6a. None of these curves matches the experimental LDOS obtained either in the centre of iron island or on its rim. Therefore, we excluded this model from our consideration. Next we assumed fcc Fe with layer-wise antiferromagnetic order. The corresponding LDOS is presented in Fig. 6b. The experimental LDOS, measured in the centre of an island, agrees well with those theoretical LDOS, which were calculated for interlayer distances smaller than the $d_{Cu}$, interlayer distance in the ideal Cu(111) fcc structure. The best fit was obtained for $d_s = 0.96 d_{Cu}$, which corresponds to a surface relaxation of 4% towards the bulk.

To describe the experimental results obtained for the rim of the islands we used the structural model suggested by Biedermann *et al.* [1], in which the Fe surface layer is reconstructed into a bcc (110) structure. The theoretical LDOS, calculated for interlayer distances $d_s > d_{Cu}$ in the ferromagnetic configuration, fit the experimental STM spectra well (Fig. 6c).


[1] Biedermann, A., Rupp, W., Schmid, M. & Varga, P. Coexistence of fcc- and bcc-like crystal structures in ultrathin Fe films grown on Cu(111). *Phys. Rev. B* **73**, 165418 (2006).

[2] Berger, H. F. & Rendulic, K. D. Nozzle beam experiments on the adsorption system hydrogen/iron. *Surface Science Letters* **251-252**, A365–A365 (1991).

[3] Lisowski, W. Kinetics of hydrogen adsorption and desorption on thin platinum films. *Applied Surface Science* **31**, 451–459 (1988).

[4] Simmons, J. G. Generalized Formula for the Electric Tunnel Effect between Similar Electrodes Separated by a Thin Insulating Film. *Journal of Applied Physics* **34**, 1793 (1963).